AGU PUBLICATIONS

Geophysical Research Letters

RESEARCH LETTER
10.1002/2016GL071151

Key Points:
- The zeta potential decreases with increasing temperature at low salinity but is independent of temperature at high salinity
- At low salinity, the equilibrium calcium concentration increases with temperature but is independent of temperature at high salinity
- The temperature dependence of the zeta potential is explained by the temperature dependence of the equilibrium calcium concentration

Supporting Information:
- Supporting Information S1

Correspondence to:
D. Al Mahrouqi,
d.al-mahrouqi12@imperial.ac.uk

Citation:
Al Mahrouqi, D., J. Vinogradov, and M. D. Jackson (2016), Temperature dependence of the zeta potential in intact natural carbonates, *Geophys. Res. Lett.*, *43*, 11,578–11,587, doi:10.1002/2016GL071151.

Received 7 SEP 2016
Accepted 1 NOV 2016
Accepted article online 4 NOV 2016
Published online 17 NOV 2016

©2016. American Geophysical Union. All Rights Reserved.

Temperature dependence of the zeta potential in intact natural carbonates

Dawoud Al Mahrouqi[1,2], Jan Vinogradov[1,3], and Matthew D. Jackson[1]

[1]Department of Earth Science and Engineering, Imperial College London, London, UK, [2]Petroleum Development Oman, Muscat, Oman, [3]Now at School of Engineering, King's College, University of Aberdeen, Aberdeen, UK

Abstract The zeta potential is a measure of the electrical charge on mineral surfaces and is an important control on subsurface geophysical monitoring, adsorption of polar species in aquifers, and rock wettability. We report the first measurements of zeta potential in intact, water-saturated, natural carbonate samples at temperatures up to 120°C. The zeta potential is negative and decreases in magnitude with increasing temperature at low ionic strength (0.01 *M* NaCl, comparable to potable water) but is independent of temperature at high ionic strength (0.5 *M* NaCl, comparable to seawater). The equilibrium calcium concentration resulting from carbonate dissolution also increases with increasing temperature at low ionic strength but is independent of temperature at high ionic strength. The temperature dependence of the zeta potential is correlated with the temperature dependence of the equilibrium calcium concentration and shows a Nernstian linear relationship. Our findings are applicable to many subsurface carbonate rocks at elevated temperature.

1. Introduction

The zeta potential is a measure of the electrical charge on a mineral surface. The value of the zeta potential controls the magnitude and polarity of the streaming potential, a component of the self-potential (SP) that arises in response to pressure gradients across water saturated rocks [e.g., *Jouniaux and Pozzi*, 1995; *Schoemaker et al.,* 2012; *Luong and Sprik*, 2013; *Jackson*, 2015]. SP measurements are widely used in geophysical monitoring of fluid flow in aquifers, hydrocarbon reservoirs, and geothermal fields [e.g., *Corwin and Hoover*, 1979; *Morgan et al.,* 1989; *Wurmstich and Morgan*, 1994; *Revil and Pezard*, 1998; *Darnet et al.,* 2003; *Darnet et al.,* 2004; *Jardani et al.,* 2008; *Suski et al.,* 2008; *Bolève et al.,* 2009], and the zeta potential is an important material property used when interpreting these data (see *Jackson* [2015] for an overview). The zeta potential also controls the magnitude and polarity of the seismoelectric response [e.g., *Pride*, 1994; *Schoemaker et al.,* 2012; *Grobbe et al.,* 2014; *Grobbe and Slob*, 2016]. Rock wettability is strongly controlled by the zeta potential [e.g., *Buckley et al.,* 1989; *Strand et al.,* 2006; *Hiorth et al.,* 2010; *Jackson et al.,* 2012] and subsurface engineering processes, such as modifying the composition of injection brine during waterflooding of hydrocarbon reservoirs, are affected by its value [e.g., *Strand et al.,* 2006; *Zhang et al.,* 2007; *Yousef et al.,* 2011; *Mahani et al.,* 2016]. Adsorption and exchange of polar species on the mineral surfaces in aquifers is also influenced by the zeta potential [e.g., *Appelo*, 1994]. Consequently, knowledge of the zeta potential at conditions relevant to natural subsurface systems has broad application.

In many subsurface settings, including hydrocarbon reservoirs [e.g., *Gulamali et al.,* 2011; *Saunders et al.,* 2012], deep saline aquifers [e.g., *Guichet et al.,* 2006] and hydrothermal systems [e.g., *Revil and Pezard*, 1998; *Suski et al.,* 2008], there are carbonate rocks at elevated temperature (typically > 60°C), yet the temperature dependence of the zeta potential in carbonates remains poorly understood [*Glover*, 2015]. No measurements above laboratory temperature are available in the literature. The aim of this paper is to determine the temperature dependence of the zeta potential in natural carbonates for the first time over the range 22–120°C. We investigate three different natural limestone samples (Table S1 in the supporting information) saturated with two different electrolytes. One electrolyte contains 0.01 *M* (1 $M = 1$ mol dm^{-3}) NaCl (total ionic strength comparable to potable water); the second contains 0.5 *M* NaCl (total ionic strength comparable to seawater). Both electrolytes contain Ca^{2+} and other ions, such as Mg^{2+} and SO_4^{2-}. These are not added to the electrolyte as salts. Rather, they are present as a consequence of dissolution and exchange with the carbonate minerals during equilibration of the electrolyte-rock system at the temperature of interest, prior to measuring the zeta potential.

2. Materials and Methods

We measured the zeta potential of the intact limestone samples using the streaming potential method (SPM) at elevated temperature recently developed by *Vinogradov and Jackson* [2015] and applied by them to intact sandstone samples. Their experimental setup was modified from that described by *Jaafar et al.* [2009] and *Vinogradov et al.* [2010] to allow measurements at elevated temperature (see Figure S1 in the supporting information). As the SPM has been described previously, we provide only a short overview here.

The sample was confined in a polyether ether ketone (PEEK) core holder and placed in an oven along with the reservoirs (columns) that supply electrolyte to the sample, and the electrodes used to measure the electrical potential across the sample. The oven had temperature controlled to $\pm$0.5°C. The pump used to flow the electrolyte through the sample remained outside of the oven and multipar oil was used as a hydraulic fluid to force electrolyte from one reservoir, through the sample, and into the other reservoir, via flow lines that pass through the wall of the oven from the reservoirs to the pump. A backpressure was applied to the fluids in the reservoirs of approximately 50 kPa above the temperature-dependent water boiling pressure.

For temperatures in the range 22–80°C, the electrolyte pH, electrical conductivity, and concentrations of key ions were measured using samples obtained inside the oven; measurements at higher temperature were not possible. However, the zeta potential and the electrical conductivity of the saturated rock sample were measured over the entire temperature range investigated.

The streaming potential was measured using the "paired-stabilization" (PS) method of *Vinogradov and Jackson* [2011]. In this method, the pump is used to flow the electrolyte through the sample at constant rate until stable pressure and voltage are recorded across the sample (e.g., Figure 1a). Stable pressure and voltage indicate that a steady state has been reached at which the streaming current induced by the flow is balanced by a conduction current so the total current in the sample is zero across any cross section perpendicular to the induced pressure gradient. The streaming potential can only be interpreted to yield the zeta potential once this steady state is reached. The flow direction is then reversed at the same rate. The voltage change is checked to have the same magnitude but opposite polarity in response to flow in each direction, confirming that electrode polarization effects are small [e.g., *Ball and Fuerstenau*, 1973] and that the measured electrical potential corresponds to the streaming potential. These PS experiments are repeated at three or four different flow rates and the stabilized voltage for each experiment plotted as a function of the stabilized pressure difference [e.g., *Jouniaux and Pozzi*, 1995; *Lorne et al.,* 1999; *Schoemaker et al.,* 2012; *Luong and Sprik*, 2013] (see Figure 1b). The gradient of a linear regression through these data yields the streaming potential coupling coefficient (C_{sp}), which is related to the zeta potential (ζ) via a modified version of the Helmholtz-Smoluchowski equation that accounts for surface electrical conductivity [e.g., *Fairbrother and Mastin*, 1924; *Jouniaux and Pozzi*, 1995; *Revil et al.,* 1999; *Glover*, 2015].

$$C_{sp} = \frac{\Delta V}{\Delta P} = \frac{\zeta \varepsilon}{\mu_w \sigma_r F}. \quad (1)$$

Here μ_w is the dynamic viscosity of the electrolyte, ε is the permittivity of the electrolyte, σ_r is the conductivity of the sample saturated with the electrolyte at experimental conditions, and F is the intrinsic formation factor of the sample. Similar to *Vinogradov and Jackson* [2015], we obtained μ and ε as a function of temperature and ionic strength using the approach of *Saunders et al.* [2012, Appendix A], and the electrical conductivity of the saturated sample σ_r was measured before and after each streaming potential measurement using the approach reported in *Vinogradov et al.* [2010] (Figure 1c). The intrinsic formation factor F at 22°C along with other key data for the Portland, Estaillades, and Ketton samples investigated was available from previous studies [*Alroudhan et al.*, 2016] (see Table S1 in the supporting information). All three samples are pure limestone and appear compositionally similar in X-ray diffraction measurements.

The main difference in our approach compared to *Vinogradov and Jackson* [2015] was in the preparation of the samples and electrolytes prior to the measurement of zeta potential. The limestone samples were cleaned following the procedure outlined in *Alroudhan et al.* [2016]. Each sample was flooded with at least two pore volumes (PV) of deionized water prior to cleaning with methanol in a Soxhlet apparatus for 48 h and then dried for at least 12 h in a vacuum oven at 80°C. It was then allowed to cool at room temperature for a minimum of 6 h and flooded with a further 4 PV of 0.05 *M* NaCl electrolyte that had been equilibrated

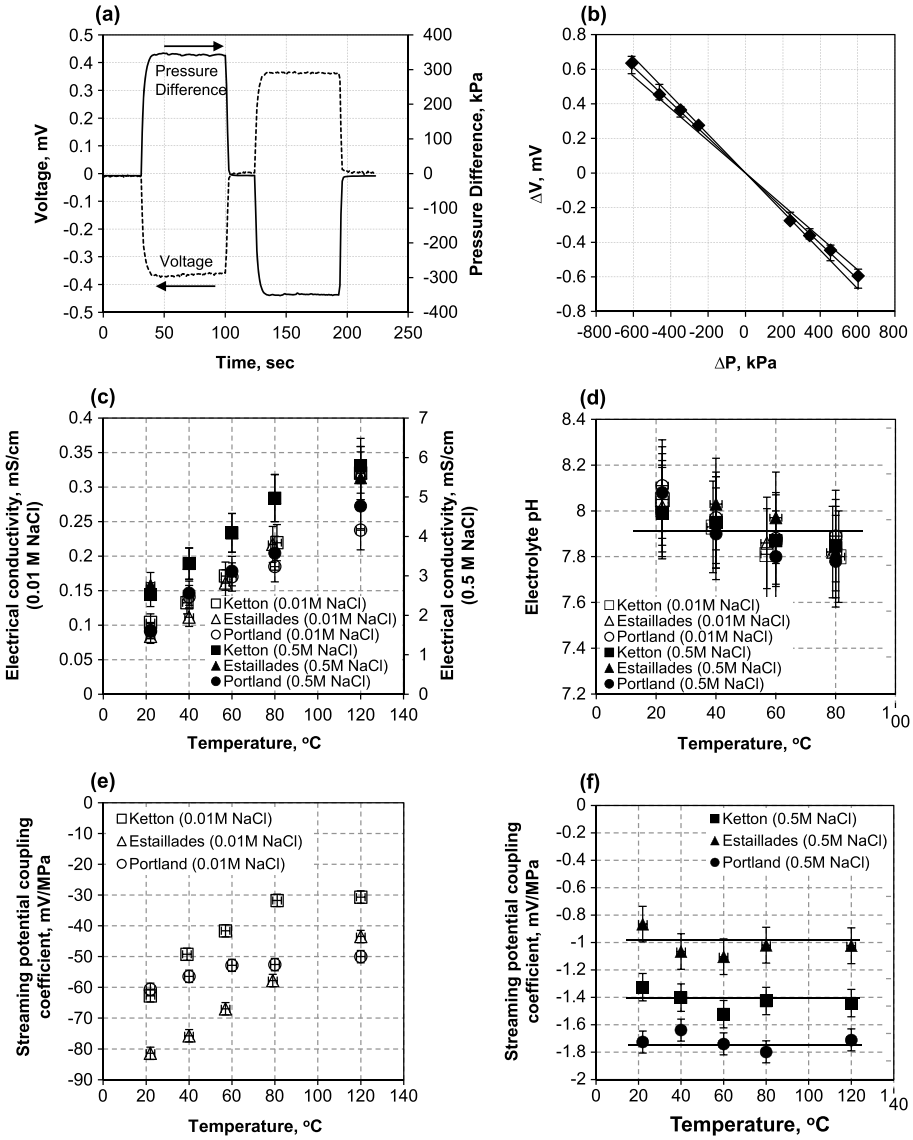


Figure 1. Experimental results. (a) Typical paired stabilization results obtained at a flow rate of 80 mL min^{-1} on the Estaillades sample saturated with 0.5 *M* NaCl electrolyte at 80°C. (b) Typical plot of stabilized voltage against stabilized pressure difference at four different flow rates; here the linear regression has adjusted $R^2 = 0.998$. The slope of the linear regression yields C_{sp}. (c) Electrical conductivity of the saturated samples as a function of temperature: filled symbols denote 0.5 *M* NaCl electrolyte and are plotted against the right-hand axis; empty symbols denote 0.01 *M* NaCl electrolyte and are plotted against the left-hand axis. (d) Electrolyte pH as a function of temperature: filled symbols denote 0.5 *M* NaCl electrolyte; empty symbols denote 0.01 *M* NaCl electrolyte. Error bars on pH reflect the instrument accuracy (±0.2 pH units). (e and f) show streaming potential coupling coefficient as a function of temperature for 0.01 M NaCl electrolyte (Figure 1e) and 0.5 M NaCl electrolyte (Figure 1f).

with the carbonate samples (see below). This enhanced cleaning protocol ensures that divalent ions have been flushed from the mineral surfaces.

Carbonate minerals are soluble in aqueous solutions, with calcite having a solubility product $K_{sp} = 10^{-8.48}$ *M* [*Plummer and Busenberg*, 1982]. Equilibrium between carbonate minerals in contact with aqueous electrolyte is defined by the pH, the concentration of the soluble ionic species and, in open system conditions, the partial pressure of CO_2 (pCO_2) in solution [*Somasundaran et al.,* 1985; *Somasundaran*, 2006]. The equilibrium pH of water in contact with calcite in the presence of CO_2 is 8.2–8.4 [*Garrels and Christ*, 1965; *Stumm and Morgan*, 1996]. Any factor, such as organic activity, CO_2 partial pressure, or temperature that modifies the equilibrium will result in precipitation or dissolution of calcite.

The appropriate equilibrium conditions for a natural carbonate/water/CO_2 system were replicated here following the approach described in *Alroudhan et al.* [2016]. In this approach, NaCl electrolytes were prepared and then placed in a closed beaker at room temperature with offcuts of the tested carbonate, maintaining an air layer in the beaker to provide a source of atmospheric CO_2, for 4–8 weeks with regular testing to determine whether equilibrium has been achieved. This mimics the open system conditions under which most carbonate rocks are initially formed [*Morse*, 1986; *Morse and Mackenzie*, 1990; *Stumm and Morgan*, 1996]. Previous studies of these samples have shown that equilibrium is reached at a measured pH of 8.2 ± 0.2 [see *Alroudhan et al.,* 2016], consistent with previous measured and calculated values [*Garrels and Christ*, 1965]. These electrolytes, equilibrated initially at open system conditions and room temperature, were used to saturate the limestone samples.

The samples were then loaded into the SPM apparatus described above. This is closed to the atmosphere and mimics the closed-system conditions pertaining to a rock-brine system at depth. The temperature was then raised to the desired value, and equilibrium of the rock/water system at this temperature and closed conditions was established by pumping the electrolyte through the sample from one reservoir to the other and back again. At regular intervals, the electrical conductivity and pH of the electrolyte in the reservoirs was measured, and equilibrium was assumed to have been reached when the conductivity and pH of the electrolyte in each reservoir differed by $<5\%$.

Electrolyte pH was measured using a Five-Go Mettler-Toledo pH meter with their 3-in-1 pH electrode LE438, implementing where necessary the manufacturer's recommended calibration and correction procedures at high ionic strength. The concentration of Ca^{2+}, Mg^{2+}, and SO_4^{2-} was measured, for temperatures in the range 22–80°C, using a Metrohm 930 ion chromatographer. Electrolyte samples were diluted to obtain concentrations between 2 and 200 pmm, and the instrumental error was assessed by running certified standard solutions contain Ca^{2+}, Mg^{2+}, and SO_4^{2-}. Repeatability was determined by conducting five repeat measurements on all the samples whose standard deviation is represented by the error bars. The errors were found to be small: 3.5% for Ca^{2+} and Mg^{2+} and 0.5% for SO_4^{2-}.

3. Results

Typical raw results of the PS experiments are shown in Figures 1a and 1b. The uncertainty in the streaming potential coupling coefficient arising from the range of linear regressions that can be forced through the stabilized voltage and pressure data was used to determine the associated experimental error in the reported zeta potentials. Figures 1c and 1d show the measured sample electrical conductivity and electrolyte pH for all experiments over the range of temperatures investigated. The sample conductivity increases with temperature almost linearly (Figure 1c), and the conductivity also increases with the electrolyte ionic strength; the higher the electrolyte concentration, the higher the conductivity. Electrolyte pH is constant within experimental error in all investigated samples and electrolytes (Figure 1d). Figures 1e and 1f show the temperature-dependent change in streaming potential coupling coefficient for the 0.01 *M* and 0.5 *M* electrolytes, respectively. The streaming potential coupling coefficient is negative for all samples and decreases in magnitude with increasing temperature at low ionic strength (Figure 1e) but is constant within experimental error at high ionic strength (Figure 1f).

Figure 2 shows the temperature dependence of the zeta potential and calcium concentration (expressed as *p*Ca, where *p* denotes the negative logarithm; higher *p*Ca corresponds to lower Ca^{2+} concentration and vice versa) for the 0.01 *M* (Figures 2a and 2b) and 0.5 *M* (Figures 2c and 2d) electrolytes. Plotting calcium concentration in this way is analogous to plotting the proton concentration as pH, although we do not account for the nonideal nature of the electrolyte (i.e., we plot the negative logarithm of calcium concentration rather than activity).

At low ionic strength, zeta potential and calcium concentration both increase with increasing temperature (Figures 2a and 2b). A linear regression provides a good fit to the temperature dependence of the zeta potential for the Estaillades and Portland samples with a common gradient of 0.04 mV/°C (adjusted $R^2 = 0.897$ for Estaillades and adjusted $R^2 = 0.974$ for Portland), but a power law regression of the form $a = bT^c$ is required to obtain a similar quality of fit to the data from the Ketton sample (adjusted $R^2 = 0.958$) with $b = -41.46$ mV and $c = -0.409$. A linear regression also provides a good fit to the temperature dependence

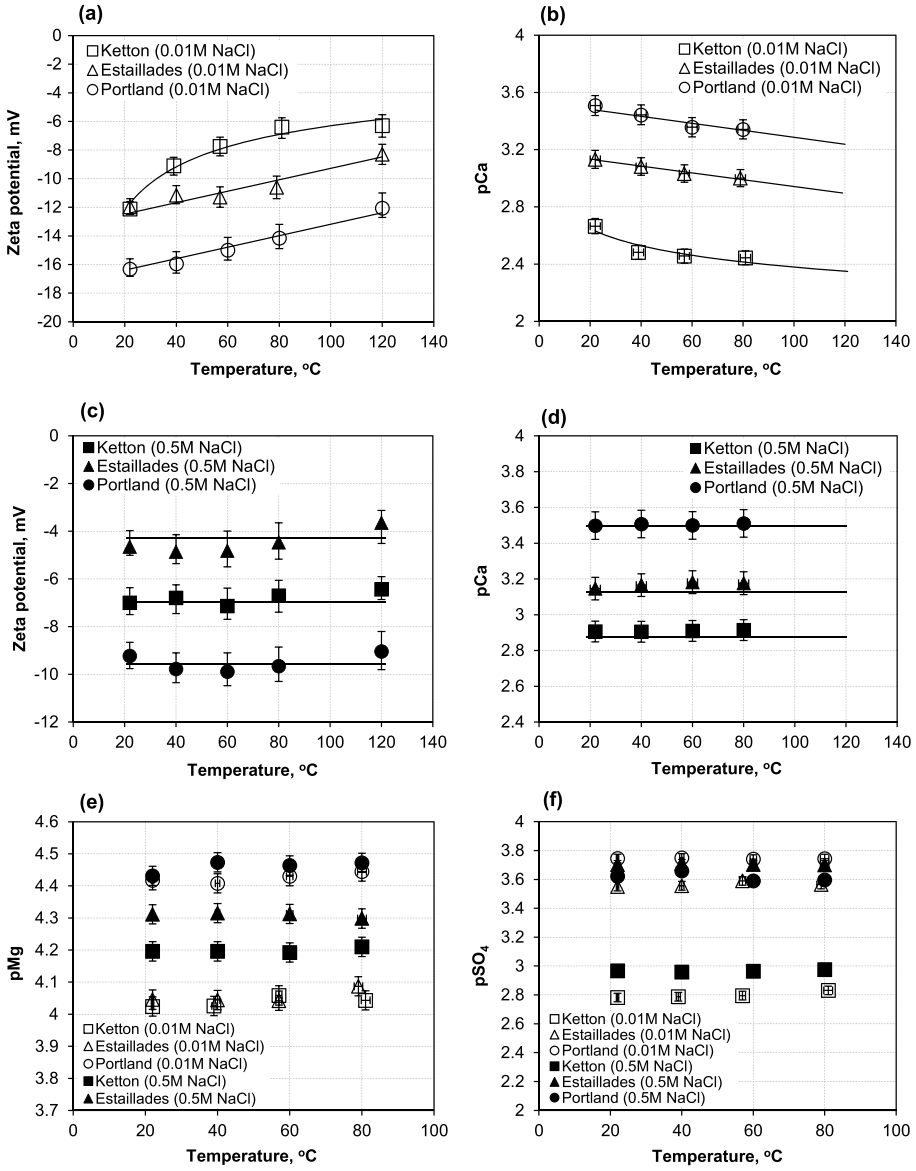


Figure 2. Zeta potential and equilibrium *p*Ca, *p*Mg, and pSO_4 as a function of temperature. (a and b) Zeta potential and *p*Ca as a function of temperature at low ionic strength (0.01 *M* NaCl electrolyte). (c and d) Zeta potential and *p*Ca as a function of temperature at high ionic strength (0.5 *M* NaCl electrolyte). The equilibrium *p*Ca was measured for temperatures in the range 22–80°C and extrapolated to higher temperature using the regressions obtained. (e and f) *p*Mg and pSO_4 as a function of temperature for all samples and electrolytes.

of *p*Ca for the Estaillades and Portland samples with a common gradient of −0.0024 decade/°C (adjusted $R^2 = 0.977$ for Estaillades and adjusted $R^2 = 0.896$ for Portland), but again, a power law regression is required to obtain a similar quality of fit to the data from the Ketton sample (adjusted $R^2 = 0.844$) with $b = 3.23$ and $c = -0.067$. The absolute magnitude of the zeta potential and calcium concentration (expressed as *p*Ca) for each sample consistently follows the order Portland > Estaillades > Ketton.

At high ionic strength, both zeta potential and calcium concentration are independent of temperature within experimental error (Figures 2c and 2d). The absolute magnitude of the zeta potential for each sample consistently follows the order Portland > Ketton > Estaillades (Figure 2c). However, the calcium concentration (expressed as *p*Ca) follows the order Portland > Estaillades > Ketton (Figure 2d). Dissolution of the sample during equilibrium of the rock/electrolyte system therefore yielded a nonzero concentration of Ca^{2+} in the electrolyte that was temperature dependent at low ionic strength, but constant for a given sample at high

ionic strength. The equilibration process also yielded nonzero concentrations of Mg^{2+} and SO_4^{2-} which were independent of temperature irrespective of ionic strength, but varied between samples (Figures 2e and 2f). The difference in equilibrium *p*Mg between the three samples is small and follows the trend in *p*Ca, so *p*Mg is lower in the Ketton sample and higher in the Portland sample; see Figure 2e). The equilibrium pSO_4 is always lower in the Ketton sample (Figure 2f), consistent with previous results obtained at room temperature. We discuss the significance of these ions in solution in terms of their impact on zeta potential in the next section.

4. Discussion

We observe a clear and consistent temperature dependence of the zeta potential in natural carbonates which is the same across the three different limestone samples investigated here but depends on the ionic strength of the electrolyte. At the lower ionic strength tested (0.01 *M* NaCl), the zeta potential decreases in magnitude with increasing temperature, while at the higher ionic strength tested (0.5 *M* NaCl), the zeta potential remains constant within experimental error. This behavior is similar to that observed in natural sandstones by *Vinogradov and Jackson* [2015]; they also found that the zeta potential decreased in magnitude with increasing temperature at lower ionic strength (0.01 *M* NaCl, consistent with that investigated here) but remained constant at higher ionic strength (0.5 *M* NaCl, as in this study). However, they found that the zeta potential at a given temperature was the same within experimental error across the three sandstone samples investigated. Moreover, they also found that the electrolyte pH decreased in magnitude with increasing temperature at low ionic strength but remained constant at high ionic strength. Here we find the value of zeta potential is different for each limestone sample. Moreover, the pH remained constant within experimental error, irrespective of temperature or ionic strength.

The negative values of zeta potential obtained here for all three carbonate samples investigated are consistent with previously reported values on natural carbonates and calcites at the equilibrium pH = 8.2 [e.g., *Berlin and Khabakov*, 1961]. However, there are no published data on the temperature dependence of the zeta potential on calcite or natural carbonates against which the results obtained here can be compared. All previously published data were obtained at laboratory temperature [e.g., *Foxall et al.,* 1979; *Thompson and Pownall*, 1989; *Pierre et al.,* 1990; *Huang et al.,* 1991; *Cicerone et al.,* 1992; *Chen et al.,* 2014; *Alroudhan et al.,* 2016]. These studies have shown that unlike metal oxides such as silica [e.g., *Glover et al.,* 2012], the proton is not the key potential determining ion (PDI; being those ions whose concentration in aqueous solution controls the polarity and density of electrical charge on the mineral surface) for the calcite surface. While pH does control the protonation and deprotonation reactions that occur at the calcite mineral surface, the variation in surface charge over the pH range 5.5–11 is small [e.g., *Heberling et al.*, 2011].

The zeta potential is instead controlled by the concentration-dependent adsorption of the lattice ions Ca^{2+} and Mg^{2+} on the mineral surface. Many authors have concluded that Ca^{2+} and Mg^{2+} are the principle PDIs [e.g., *Somasundaran and Agar*, 1967; *Foxall et al.,* 1979; *Pierre et al.,* 1990; *Huang et al.,* 1991; *Cicerone et al.,* 1992; *Stipp*, 1999; *Moulin and Roques*, 2003; *Wolthers et al.,* 2008; *Heberling et al.,* 2011; *Alroudhan et al.,* 2016]. The consistent observation in these studies is that decreasing *p*Ca and/or *p*Mg yield more positive zeta potential, consistent with increased adsorption of Ca^{2+} and/or Mg^{2+} onto the calcite surface. The SO_4^{2-} ion has also been suggested as a PDI for calcite [e.g., *Smallwood*, 1977; *Strand et al.,* 2006]. The zeta potential of the natural limestone samples investigated here is therefore controlled by *p*Ca, *p*Mg, and pSO_4; i.e., the concentration of Ca^{2+}, Mg^{2+}, and SO_4^{2-}.

The equilibrium *p*Mg and pSO_4 observed in our experiments was constant for a given sample and electrolyte irrespective of temperature (Figures 2e and 2f). At the higher ionic strength tested, the equilibrium *p*Ca was also constant for a given sample and electrolyte irrespective of temperature (Figure 2d). However, at the lower ionic strength tested, the equilibrium *p*Ca decreased with increasing temperature (i.e., the concentration of Ca^{2+} increased; Figure 2b). Moreover, at the lower ionic strength, a clear correlation between zeta potential and *p*Ca was obtained for a given sample, yielding a linear (Nernstian) regression with a gradient of −15 mV/decade for the Portland and Estaillades samples (adjusted $R^2 > 0.91$) and −20 mV/decade for the Ketton sample (adjusted $R^2 = 0.90$) (Figure 3a). Previous studies on the same carbonate samples investigated here [e.g., *Alroudhan et al.,* 2016] and on calcite samples in NaCl/KCl electrolytes at low ionic strength ($<2\times10^{-2}$ *M*) have also observed a Nernstian relationship between zeta potential and *p*Ca with similar

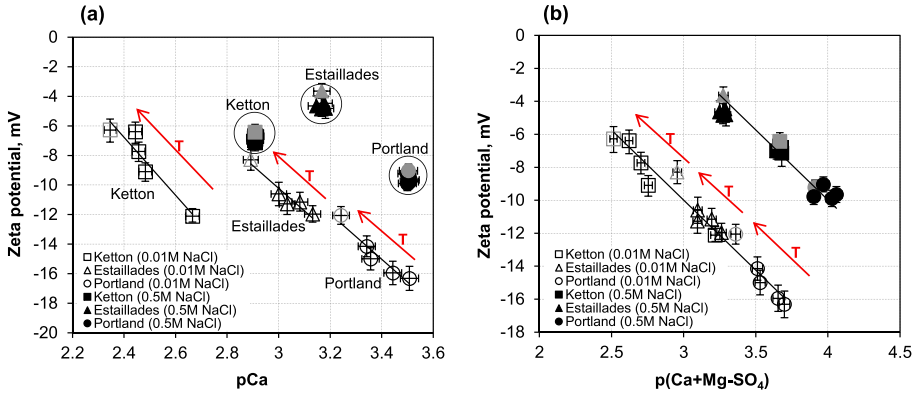


Figure 3. Relationship between zeta potential and PDI concentration. (a) Zeta potential plotted against *p*Ca. (b) Zeta potential plotted against $p(Ca + Mg\text{-}SO_4)$. Red arrows represent increasing temperature from 22°C to 120°C. Grey symbols are extrapolated values at 120°C.

gradient but at fixed (laboratory) temperature [*Foxall et al.*, 1979; *Thompson and Pownall*, 1989; *Cicerone et al.*, 1992]; see Figure S2 in the supporting information. At the higher ionic strength, the data clustered at one value of *p*Ca and zeta potential for each sample (Figure 3a).

The temperature dependence of the zeta potential in sandstones observed by *Vinogradov and Jackson* [2015] was explained by them in terms of the temperature dependence of the electrolyte pH (i.e., the concentration of the proton and the PDI for the silica surface). Here we find that the temperature dependence of the zeta potential for a given carbonate sample can be explained by the temperature dependence of the electrolyte *p*Ca (i.e., the concentration of the calcium ion and a PDI for the calcite surface). At the lower ionic strength investigated, both the zeta potential and *p*Ca decrease (i.e., the concentration of Ca^{2+} increases) with increasing temperature (Figures 2a and 2b) and the change in zeta potential reflects a Nernstian response to the change in *p*Ca (Figure 3a). At the higher ionic strength investigated, both the zeta potential and *p*Ca remain constant irrespective of temperature (Figures 2c and 2d) but the constant zeta potential nonetheless reflects a Nernstian response to the change in *p*Ca (Figure 3a).

The relationship between zeta potential and equilibrium *p*Ca explains the temperature dependence of the zeta potential for a given limestone sample but does not explain the difference in zeta potential observed at a given *p*Ca/temperature between the three investigated limestone samples. For example, the Ketton sample recorded a larger negative zeta potential than the Estaillades sample at high ionic strength, even though the calcium concentration was higher (i.e., *p*Ca was lower; see Figure 3a). The difference in zeta potentials can be accounted for by also including the variations in equilibrium *p*Mg and pSO_4 observed across the different samples (Figures 2e and 2f). The difference in the zeta potential response of the three samples tested can be accounted for by plotting the zeta potential against the total concentration of PDIs (expressed as $p(Ca + Mg\text{-}SO_4)$). We choose to plot concentration in this way as the lattice ions Ca^{2+} and Mg^{2+} have an identical impact on zeta potential within experimental error, while the SO_4^{2-} ion acts to reduce the effect of pCa [see *Alroudhan et al.*, 2016]. Plotted in this way, the zeta potential varies linearly with PDI concentration irrespective of sample type, temperature, and ionic strength, with an identical gradient of -8 mV/decade (adjusted $R^2 > 0.93$) (Figure 3b).

A simple but plausible mechanism to account for the observed temperature dependence of *p*Ca and zeta potential is variable carbonate dissolution during the equilibration process caused by temperature-dependent changes in pH. At low ionic strength, the pH has been observed to decrease with temperature in unbuffered NaCl electrolytes [e.g., *Millero et al.*, 2009; *Vinogradov and Jackson*, 2015]; however, the pH in our closed-system experiments is buffered at the equilibrium value as a consequence of carbonate dissolution leading to a decrease in *p*Ca (Figure 2b). At high ionic strength, *Vinogradov and Jackson* [2015] observed no change in pH with temperature. Hence, we expect no mineral dissolution and so no change in *p*Ca (Figure 2d).

The relationships between zeta potential, temperature, and *p*Ca reported in this study are important for many subsurface applications. For example, carbonate hydrothermal fields and many deep carbonate hydrocarbon

reservoirs or potential CO_2 storage sites are at temperatures >60°C and, as discussed in section 1, the zeta potential is an important parameter impacting geophysical monitoring of flow in these reservoirs, as well as interactions between the mineral surfaces and adjacent fluids. We show here that the temperature dependence of the zeta potential is specific to a given carbonate and depends on the electrolyte ionic strength and the concentration of the PDIs Ca^{2+}, Mg^{2+}, and SO_4^{2-}. In carbonate reservoirs saturated with brines of low ionic strength, the zeta potential of the mineral surfaces at depth, where temperatures are elevated, will be smaller in magnitude than values measured on reservoir samples in experiments at laboratory conditions. Moreover, measurements of equilibrium electrolyte composition, especially the concentration of Ca^{2+}, Mg^{2+}, and SO_4^{2-}, are essential to predict correctly the zeta potential at depth. However, in carbonate reservoirs saturated with brines of high ionic strength, the zeta potential will be independent of temperature and, for a given carbonate type, zeta potential measurements on samples at laboratory conditions may be directly applied to the reservoir at depth.

5. Conclusions

We find that the temperature dependence of the zeta potential in natural carbonates saturated with equilibrated NaCl electrolytes (i.e., containing Ca^{2+}, Mg^{2+}, and SO_4^{2-} ions at concentrations established during equilibrium of sample and electrolyte) is sample specific and depends on the ionic strength of the electrolyte. The zeta potential is negative and decreases in magnitude with increasing temperature at low ionic strength (represented by the 0.01 *M* NaCl electrolyte investigated here) but is independent of temperature at high ionic strength (represented by the 0.5 *M* NaCl electrolyte investigated here). This behavior is consistent with zeta potential data in intact natural sandstones. The equilibrium calcium concentration (expressed as *p*Ca) in the electrolyte also decreases with increasing temperature at low ionic strength but is independent of temperature at high ionic strength. The temperature dependence of the zeta potential can be correlated with the temperature dependence of the equilibrium *p*Ca and shows a Nernstian linear relationship. The difference in response of the carbonate samples tested can be accounted for by including sample-dependent variations in equilibrium *p*Mg and pSO_4 as well as the temperature-dependent variation in equilibrium *p*Ca. The pH remains unchanged with temperature irrespective of ionic strength. The results have broad application to processes in subsurface carbonate rocks at elevated temperature.

Acknowledgments

Supporting data are included in Word and Excel files; any additional data may be obtained from the corresponding author (e-mail: d.al-mahrouqi12@imperial.ac.uk). TOTAL are thanked for partially funding Jackson under the TOTAL Chairs programme at Imperial College London and for supporting the activities of the TOTAL Laboratory for Reservoir Physics at Imperial College where the experiments reported were conducted. Petroleum Development Oman is thanked for supporting Al Mahrouqi.

References

Alroudhan, A., J. Vinogradov, and M. Jackson (2016), Zeta potential of intact natural limestone: Impact of potential-determining ions Ca, Mg and SO_4, *Colloids Surf. A*, *493*, 83–98, doi:10.1016/j.colsurfa.2015.11.068.

Appelo, C. (1994), Cation and proton exchange, pH variations, and carbonate reactions in a freshening aquifer, *Water Resour. Res.*, *30*(10), 2793–2805, doi:10.1029/94WR01048.

Ball, B., and D. Fuerstenau (1973), A review of the measurement of streaming potentials, *Miner. Sci. Eng*, *5*(4), 267–277.

Berlin, T. S., and A. V. Khabakov (1961), Difference in the electrokinetic potentials of carbonate sedimentary rocks of different origin and composition, *Geochemistry*, *3*, 217–230.

Bolève, A., A. Revil, F. Janod, J. Mattiuzzo, and J.-J. Fry (2009), Preferential fluid flow pathways in embankment dams imaged by self-potential tomography, *Near Surf. Geophys.*, *7*(5–6), 447–462, doi:10.3997/1873-0604.2009012.

Buckley, J., K. Takamura, and N. Morrow (1989), Influence of electrical surface charges on the wetting properties of crude oils, *SPE Reservoir Eng.*, *4*(03), 332–340.

Chen, L., G. Zhang, L. Wang, W. Wu, and J. Ge (2014), Zeta potential of limestone in a large range of salinity, *Colloids Surf. A*, *450*(0), 1–8, doi:10.1016/j.colsurfa.2014.03.006.

Cicerone, D. S., A. E. Regazzoni, and M. A. Blesa (1992), Electrokinetic properties of the calcite water interface in the presence of magnesium and organic-matter, *J. Colloid Interface Sci.*, *154*(2), 423–433, doi:10.1016/0021-9797(92)90158-i.

Corwin, R. F., and D. B. Hoover (1979), The self-potential method in geothermal exploration, *Geophysics*, *44*(2), 226–245, doi:10.1190/1.1440964.

Darnet, M., G. Marquis, and P. Sailhac (2003), Estimating aquifer hydraulic properties from the inversion of surface streaming potential (SP) anomalies, *Geophys. Res. Lett.*, *30*(13), 1679, doi:10.1029/2003GL017631.

Darnet, M., A. Maineult, and G. Marquis (2004), On the origins of self-potential (SP) anomalies induced by water injections into geothermal reservoirs, *Geophys. Res. Lett.*, *31*, L19609, doi:10.1029/2004GL020922.

Fairbrother, F., and H. Mastin (1924), Studies in electro-endosmosis, *J. Chem. Soc., Trans.*, *125*, 2319–2330, doi:10.1039/CT9242502319.

Foxall, T., G. C. Peterson, H. M. Rendall, and A. L. Smith (1979), Charge determination at calcium salt/aqueous solution interface, *J. Chem. Soc., Faraday Trans. 1*, *75*, 1034–1039, doi:10.1039/F19797501034.

Garrels, R. M., and C. L. Christ (1965), *Solutions, Minerals, and Equilibria*, Harper & Row, New York.

Glover, P. (2015), Geophysical properties of the near surface earth: Electrical properties, in *Treatise on Geophysics*, vol. 11, 2nd ed., edited by G. Schubert, pp. 89–137, Elsevier, Oxford.

Glover, P. W. J., E. Walker, and M. D. Jackson (2012), Streaming-potential coefficient of reservoir rock: A theoretical model, *Geophysics*, *77*(2), D17–D43, doi:10.1190/geo2011-0364.1.

Grobbe, N., and E. Slob (2016), Seismo-electromagnetic thin-bed responses: Natural signal enhancements? *J. Geophys. Res.: Solid Earth*, *121*, 2460–2479, doi:10.1002/2015JB012381.

Grobbe, N., J. Hunziker, and E. Slob (2014), Seismoelectric wave propagation modeling for typical laboratory configurations: A numerical validation, paper presented at 2014 SEG Annual Meeting, Society of Exploration Geophysicists.
Guichet, X., L. Jouniaux, and N. Catel (2006), Modification of streaming potential by precipitation of calcite in a sand–water system: Laboratory measurements in the pH range from 4 to 12, *Geophys. J. Int.*, *166*(1), 445–460, doi:10.1111/j.1365-246X.2006.02922.x.
Gulamali, M. Y., E. Leinov, and M. D. Jackson (2011), Self-potential anomalies induced by water injection into hydrocarbon reservoirs, *Geophysics*, *76*(4), F283–F292, doi:10.1190/1.3596010.
Heberling, F., T. P. Trainor, J. Lützenkirchen, P. Eng, M. A. Denecke, and D. Bosbach (2011), Structure and reactivity of the calcite–water interface, *J. Colloid Interface Sci.*, *354*(2), 843–857, doi:10.1016/j.jcis.2010.10.047.
Hiorth, A., L. M. Cathles, and M. V. Madland (2010), The impact of pore water chemistry on carbonate surface charge and oil wettability, *Transport Porous Med.*, *85*(1), 1–21, doi:10.1007/s11242-010-9543-6.
Huang, Y. C., F. M. Fowkes, T. B. Lloyd, and N. D. Sanders (1991), Adsorption of calcium ions from calcium chloride solutions onto calcium carbonate particles, *Langmuir*, *7*(8), 1742–1748, doi:10.1021/la00056a028.
Jaafar, M. Z., J. Vinogradov, and M. D. Jackson (2009), Measurement of streaming potential coupling coefficient in sandstones saturated with high salinity NaCl brine, *Geophys. Res. Lett.*, *36*, L21306, doi: 10.1029/2009GL040549.
Jackson, M. D. (2015), Self-potential: Tools and techniques, in *Treatise on Geophysics*, vol. 11, 2nd ed., edited by G. Schubert chap. 9, Elsevier, Oxford.
Jackson, M. D., M. Y. Gulamali, E. Leinov, J. H. Saunders, and J. Vinogradov (2012), Spontaneous potentials in hydrocarbon reservoirs during waterflooding: Application to water-front monitoring, *SPE J.*, *17*(01), 53–69, doi:10.2118/135146-PA.
Jardani, A., A. Revil, A. Bolève, and J. Dupont (2008), Three-dimensional inversion of self-potential data used to constrain the pattern of groundwater flow in geothermal fields, *J. Geophys. Res.*, *113*, B09204, doi:10.1029/2007JB005302.
Jouniaux, L., and J. P. Pozzi (1995), Streaming potential and permeability of saturated sandstones under triaxial stress: Consequences for electrotelluric anomalies prior to earthquakes, *J. Geophys. Res.*, *100*, 10,197–10,209, doi:10.1029/95JB00069.
Lorne, B., F. Perrier, and J. P. Avouac (1999), Streaming potential measurements 1. Properties of the electrical double layer from crushed rock samples, *J. Geophys. Res.*, *104*, 17,857–17,877, doi:10.1029/1999JB900156.
Luong, D., and R. Sprik (2013), Streaming potential and electroosmosis measurements to characterize porous materials, *ISRN Geophys.*, *2013*, 496352, doi: 10.1155/2013/496352.
Mahani, H., A. L. Keya, S. Berg, and R. Nasralla (2016), Electrokinetics of carbonate/brine interface in low-salinity waterflooding: Effect of brine salinity, composition, rock type, and pH on ζ-potential and a surface-complexation model, *Paper SPE 181745 in SPE Journal*.
Millero, F. J., B. DiTrolio, A. F. Suarez, and G. Lando (2009), Spectroscopic measurements of the pH in NaCl brines, *Geochim. Cosmochim. Acta*, *73*(11), 3109–3114, doi:10.1016/j.gca.2009.01.037.
Morgan, F., E. Williams, and T. Madden (1989), Streaming potential properties of westerly granite with applications, *J. Geophys. Res.*, *94*, 12,449–12,461, doi:10.1029/JB094iB09p12449.
Morse, J. W. (1986), The surface chemistry of calcium carbonate minerals in natural waters: An overview, *Mar. Chem.*, *20*(1), 91–112, doi:10.1016/0304-4203(86)90068-X.
Morse, J. W., and F. T. Mackenzie (1990), *Geochemistry of Sedimentary Carbonates*, Elsevier, Oxford.
Moulin, P., and H. Roques (2003), Zeta potential measurement of calcium carbonate, *J. Colloid Interface Sci.*, *261*(1), 115–126, doi:10.1016/S0021-9797(03)00057-2.
Pierre, A., J. Lamarche, R. Mercier, A. Foissy, and J. Persello (1990), Calcium as potential determining ion in aqueous calcite suspensions, *J. Dispersion Sci. Technol.*, *11*(6), 611–635, doi:10.1080/01932699008943286.
Plummer, L. N., and E. Busenberg (1982), The solubilities of calcite, aragonite and vaterite in CO_2-H_2O solutions between 0 and 90°C, and an evaluation of the aqueous model for the system $CaCO_3$-CO_2-H_2O, *Geochim. Cosmochim. Acta*, *46*(6), 1011–1040, doi:10.1016/0016-7037(82)90056-4.
Pride, S. (1994), Governing equations for the coupled electromagnetics and acoustics of porous media, *Phys. Rev. B*, *50*(21), 15,678, doi:10.1103/PhysRevB.50.15678.
Revil, A., and P. Pezard (1998), Streaming electrical potential anomaly along faults in geothermal areas, *Geophys. Res. Lett.*, *25*, 3197–3200, doi:10.1029/98GL02384.
Revil, A., P. A. Pezard, and P. W. J. Glover (1999), Streaming potential in porous media 1. Theory of the zeta potential, *J. Geophys. Res.*, *104*, 20,021–20,031, doi:10.1029/1999JB900089.
Saunders, J. H., M. D. Jackson, M. Y. Gulamali, J. Vinogradov, and C. C. Pain (2012), Streaming potentials at hydrocarbon reservoir conditions, *Geophysics*, *77*(1), E77–E90, doi:10.1190/geo2011-0068.1.
Schoemaker, F., N. Grobbe, M. Schakel, S. De Ridder, E. Slob, and D. Smeulders (2012), Experimental validation of the electrokinetic theory and development of seismoelectric interferometry by cross-correlation, *Int. J. Geophys.*, *2012*, doi:10.1155/2012/514242.
Smallwood, P. (1977), Some aspects of the surface chemistry of calcite and aragonite Part I: An electrokinetic study, *Colloid Polym. Sci.*, *255*(9), 881–886.
Somasundaran, P. (2006), *Encyclopedia of Surface and Colloid Science*, CRC press, New York.
Somasundaran, P., and G. Agar (1967), The zero point of charge of calcite, *J. Colloid Interface Sci.*, *24*(4), 433–440.
Somasundaran, P., J. O. Amankonah, and K. Ananthapadmabhan (1985), Mineral-solution equilibria in sparingly soluble mineral systems, *Colloids Surf.*, *15*, 309–333.
Stipp, S. (1999), Toward a conceptual model of the calcite surface: Hydration, hydrolysis, and surface potential, *Geochim. Cosmochim. Acta*, *63*(19), 3121–3131, doi:10.1016/S0016-7037(99)00239-2.
Strand, S., E. J. Hognesen, and T. Austad (2006), Wettability alteration of carbonates—Effects of potential determining ions (Ca^{2+} and SO_4^{2-}) and temperature, *Colloids Surf. A*, *275*(1–3), 1–10, doi:10.1016/j.colsurfa.2005.10.061.
Stumm, W., and J. Morgan (1996), *Aquatic Chemistry, Chemical Equilibra and Rates in Natural Waters*, 3rd ed., J. Wiley, New York.
Suski, B., F. Ladner, L. Baron, F.-D. Vuataz, F. Philippossian, and K. Holliger (2008), Detection and characterization of hydraulically active fractures in a carbonate aquifer: Results from self-potential, temperature and fluid electrical conductivity logging in the Combioula hydrothermal system in the southwestern Swiss Alps, *Hydrogeol. J.*, *16*(7), 1319–1328, doi:10.1007/s10040-008-0302-5.
Thompson, D. W., and P. G. Pownall (1989), Surface electrical-properties of calcite, *J. Colloid Interface Sci.*, *131*(1), 74–82, doi:10.1016/0021-9797(89)90147-1.
Vinogradov, J., and M. D. Jackson (2011), Multiphase streaming potential in sandstones saturated with gas/brine and oil/brine during drainage and imbibition, *Geophys. Res. Lett.*, *38*, L01301, doi: 10.1029/2010GL045726.
Vinogradov, J., and M. D. Jackson (2015), Zeta potential in intact natural sandstones at elevated temperatures, *Geophys. Res. Lett.*, *42*, 6287–6294, doi:10.1002/2015GL064795.

Vinogradov, J., M. Z. Jaafar, and M. D. Jackson (2010), Measurement of streaming potential coupling coefficient in sandstones saturated with natural and artificial brines at high salinity, *J. Geophys. Res.*, *115*, B12204, doi:10.1029/2010JB007593.

Wolthers, M., L. Charlet, and P. Van Cappellen (2008), The surface chemistry of divalent metal carbonate minerals; a critical assessment of surface charge and potential data using the charge distribution multi-site ion complexation model, *Am. J. Sci.*, *308*(8), 905–941, doi:10.2475/08.2008.02.

Wurmstich, B., and F. Morgan (1994), Modeling of streaming potential responses caused by oil well pumping, *Geophysics*, *59*(1), 46–56, doi:10.1190/1.1443533.

Yousef, A. A., S. H. Al-Saleh, A. Al-Kaabi, and M. S. Al-Jawfi (2011), Laboratory investigation of the impact of injection-water salinity and ionic content on oil recovery from carbonate reservoirs, *SPE Reservoir Eval. Eng.*, *14*(05), 578–593, doi:10.2118/137634-PA.

Zhang, P., M. T. Tweheyo, and T. Austad (2007), Wettability alteration and improved oil recovery by spontaneous imbibition of seawater into chalk: Impact of the potential determining ions Ca^{2+}, Mg^{2+}, and SO_4^{2-}, *Colloids Surf. A*, *301*(1–3), 199–208, doi:10.1016/j.colsurfa.2006.12.058.